Designing donor-acceptor conjugated macrocycles with polyradical character and global aromaticity

Md Abdus Sabuj, Md Masrul Huda, & Neeraj Rai*

Dave C. Swalm School of Chemical Engineering, and Center for Advanced Vehicular Systems, Mississippi State University, MS 39762, USA.

E-mail: neerajrai@che.msstate.edu

Abstract

Polyradical character and global aromaticity are fundamental concepts that govern the rational design of cyclic conjugated macromolecules for optoelectronic applications. Here, we have designed donor-acceptor (D−A) macromolecules with ring topology along with their π-spacer derivatives, and analyzed their unique electronic properties with density functional theory (DFT). The macromolecules with $n = 8$ and 16 repeat D−A units display similar singlet–triplet energy gap and have closed-shell electronic configuration with no diradical character ($y_0 = 0$). Also, the closed-shell macromolecules display global nonaromatic character in the singlet and lowest triplet states, which is supported by NICS(0), AICD, and 2D-ICSS analysis. However, the derivatives with π-spacer ($n = 8$-π) develop near pure open-shell character ($y_0 \approx 1$) with increased singlet–triplet energy gap than the closed-shell macromolecules. Furthermore, the π-spacer derivatives display global nonaromaticity in the singlet ground-state, global aromaticity in the lowest triplet state according to Baird's rule, and have a very high polyradical character in the singlet ground-state, which is not reported for

D−A type macromolecules. The calculated absorption spectra of the open-shell macromolecules with time-dependent DFT (TDDFT) indicates intensive light absorption in the near-infrared (NIR) region broadening to 2500 nm. Also, the closed-shell macrocycles display a size-dependent absorption maxima when the number of repeat units increased from $n = 8$ to 16. Furthermore, due to the development of open-shell character in the π-spacer derivatives, a significant red-shift in the absorbance wavelength is observed than the closed-shell macromolecules.

Introduction

The π-conjugated open-shell organic semiconductor (OSCs) with one or more unpaired electrons in the degenerate or near-degenerate molecular orbitals (MOs) exhibit unique electronic, optical, and magnetic properties.[1–4] The weakly interacting unpaired electrons facilitates spin delocalization along the conjugated backbone, improving charge transfer and thermodynamic stability of the molecule.[3] Most π-conjugated materials with even numbers of electrons do not overcome the covalency between the electrons in the frontier MOs (FMOs); therefore, these have a closed-shell ground-state in the neutral form. Open-shell OSCs with di- or polyradical character are of particular interest for their potential applications as magnetic materials, for nonlinear optics, in the singlet fission process, for charge storage devices, or in organic spintronics.[4–8]

However, when it comes to designing molecules with higher radical (above diradical) characters, synthetic routes or characterization techniques are not well established. Therefore, new molecular structures are yet to be designed with significant polyradical character to understand multiple spin-spin interactions[2] with improved magnetic properties. Arrangement of an alternating donor (D) and acceptor (A) units in a conjugated system is a common approach for tuning the electronic properties of the OSCs. These D−A materials are widely used to design advanced and emerging optoelectronic devices.[9–13] Although a large number of studies have been conducted to design, synthesize, and characterize linear π-conjugated

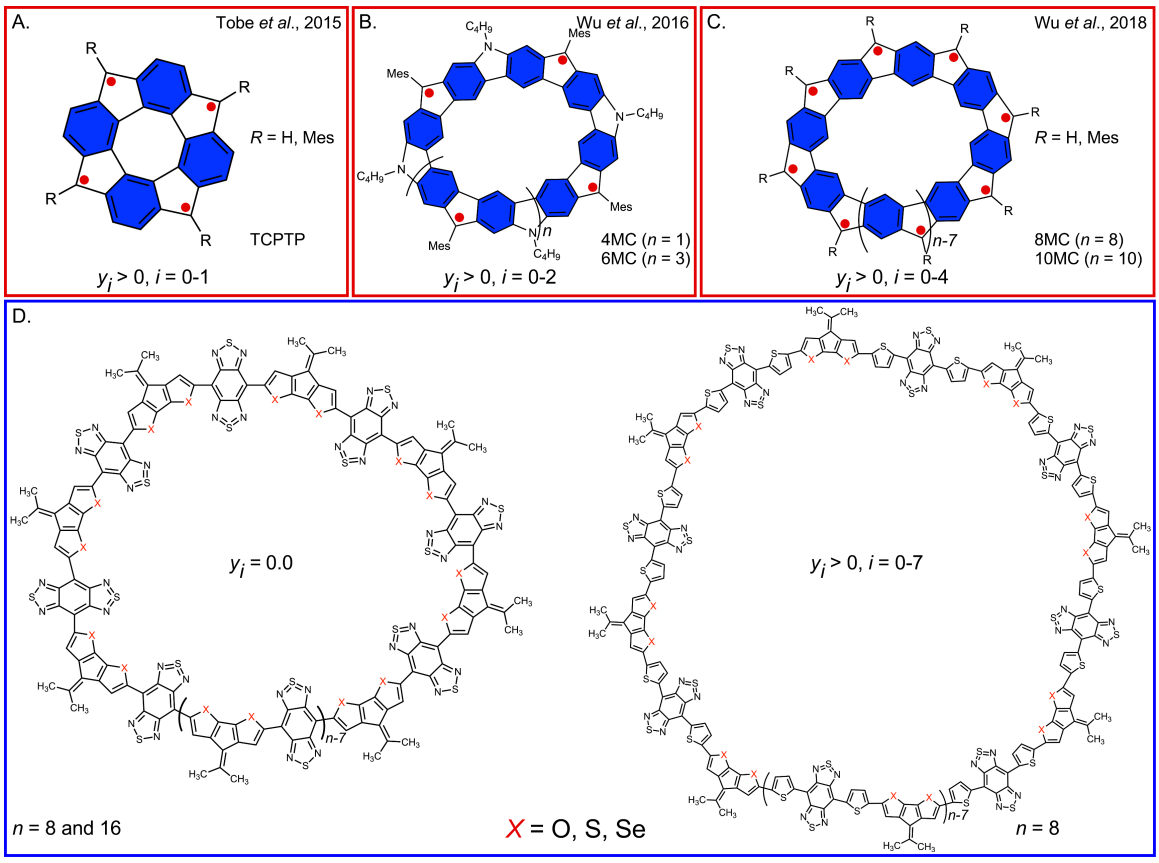

Figure 1: Prototypical examples of macromolecular polyradicaliods. (A) TCPTP with a very small tetraradical character; (B) a quinoidal/aromatic carbazole macrocycle with a moderate tetra- and hexaradical characters; (C) a annulene-within-an-annulene (AWA) super-ring structure with decaradical character; and (D) the molecular structures of CPDF-(X = O), CPDT-(X = S), and CPDS-BBT (X = Se) macromolecules with their π-spacer derivatives, having hexadecaradical character studied in this work.

D−A oligomers and polymers, very few reports are available where D−A motifs are used as a building block in π-conjugated macromolecules with the ring topology.

The traditional approach of designing a diradical molecule is to embed quinoidal units in the π-conjugated system; therefore, aromatic stabilization of these subunits overcomes the covalency of a carbon–carbon π-bond to provide the necessary potential to create two unpaired electrons.[3] Recovery of an increased number of aromatic sextet rings achieves higher driving force to develop large diradical and even polyradical character.[14] Efforts towards designing molecules with polyradical character include cyclic tetracyclopenta[*def,jkl,pqr,vwx*]-tetraphenylene (TCPTP) (Fig. 1A) and fused *p*-quinodimethane (*p*-QDM) with very small

tetraradical characters.[15,16] The reason for such a low polyradical character is the small driving force obtained from one aromatic sextet ring that is recovered from open-shell diradical to tetraradical character. Wu *et al.* have reported several π-conjugated linear and macrocyclic molecules with polyradical character.[14,17–21] They have synthesized a fully fused quinoidal/aromatic carbazole macrocycle showing a high diradical character with a moderate tetra- and hexaradical characters,[14] (Fig. 1B) and a annulene-within-an-annulene (AWA) super-ring structure with decaradical character (Fig. 1C).[19,22] This raises an important question if polyradical character can be expanded above decaradical in an alternating D−A macromolecule. Recent synthetic efforts on D−A macromolecules attempted to tune the highest occupied MO (HOMO) and lowest unoccupied MO (LUMO) energy gaps (HOMO–LUMO) by different D−A motifs to analyze optical properties.[23–31] However, cyclic D−A macromolecules with an open-shell character has not been reported in the literature.

The novel molecular architecture and delocalized spin topology of the macrocyclic molecules expanded the concept of aromaticity from an individual small ring with local aromaticity[3] to global aromaticity.[21,32] Recently, the idea of global aromaticity is explored with a 3D conjugated diradicaloid cage and a very large porphyrin nano-rings.[33,34] A highly symmetric, rigid, and extensively π-conjugated cyclic molecule displays unique global aromaticity. The cornerstone of this global aromatic character is the subtle balance between different types of antiferromagnetic (AFM) spin-spin coupling arising within the π-conjugated macrocycle backbone.[19] This complicated correlation between the AFM coupling and global aromaticity demonstrated in polycyclic aromatic hydrocarbons (PAHs),[32] but not reported for alternating D−A macrocycles.

Recently, we have reported that a particular combination of donor unit cyclopentadithiophene (CPDT) and acceptor unit thiadiazoloquinoxaline (TQ) provides a vanishing singlet–triplet energy gap upon increasing oligomer length, favoring the triplet as the ground electronic state.[3] Also, functional modification of CPDT-TQ polymer provides a wide range of electronic properties, from open-shell to closed-shell structure with a varying singlet–

triplet energy gap. Here, we have designed D−A macromolecules (Fig. 1D) with the benzo[1,2-c;4,5-c']bis[1,2,5]thiadiazole (BBT) acceptor and cyclopentadifuran (CPDF), cyclopentadithiophene (CPDT), and cyclopentadiselenophene (CPDS) donors, respectively, and followed oligomer approach to calculate their electronic properties. The choice for BBT as an acceptor is driven by its high electron affinity and the fact that it intrinsically behaves as a diradical.[35] To identify the effect of π-spacer in the macromolecules, thiophene was inserted in between the D and A units. The quinoidal nature of the heterocyclic thiophene unit regains aromatic stabilization energy in the open-shell ground-state.[36] Therefore, the macrocycles with thiophene π-spacer achieves near pure diradical character and moderate-to-high polyradical character extended to hexadecaradical (16 unpaired electrons) and global aromaticity in the lowest triplet state, following Baird's rule.[37] To the best of our knowledge, this is the first report where CPDF-, CPDT-, and CPDS-BBT is rolled to a D−A nanohoop, which shows not only a very high diradical character but also a significant polyradical character as well.

RESULTS

Optimized geometries and structural parameters

The geometry of CPDF-BBT with $n = 8$ repeat units is twisted along the backbone (Fig. 2). The twisted geometry is obtained due to a small bond length between C and O in the donor cyclopenta rings. The observed dihedral angles between a donor and adjacent acceptor unit (Fig. S1) (θ) varies between 170° to 180°. The CPDT- and CPDS-BBT form a bowl-shaped configuration, with a dihedral angle of 175°. The hoop size increases from CPDF-BBT to CPDT-BBT to CPDS-BBT due to larger C–S and C–Se bonds than the C–O bond. The CPDF-BBT macromolecule with $n = 16$ units forms a zigzag conformation to minimize energy, with an approximate distance between two adjacent D and A moieties around 5 Å.

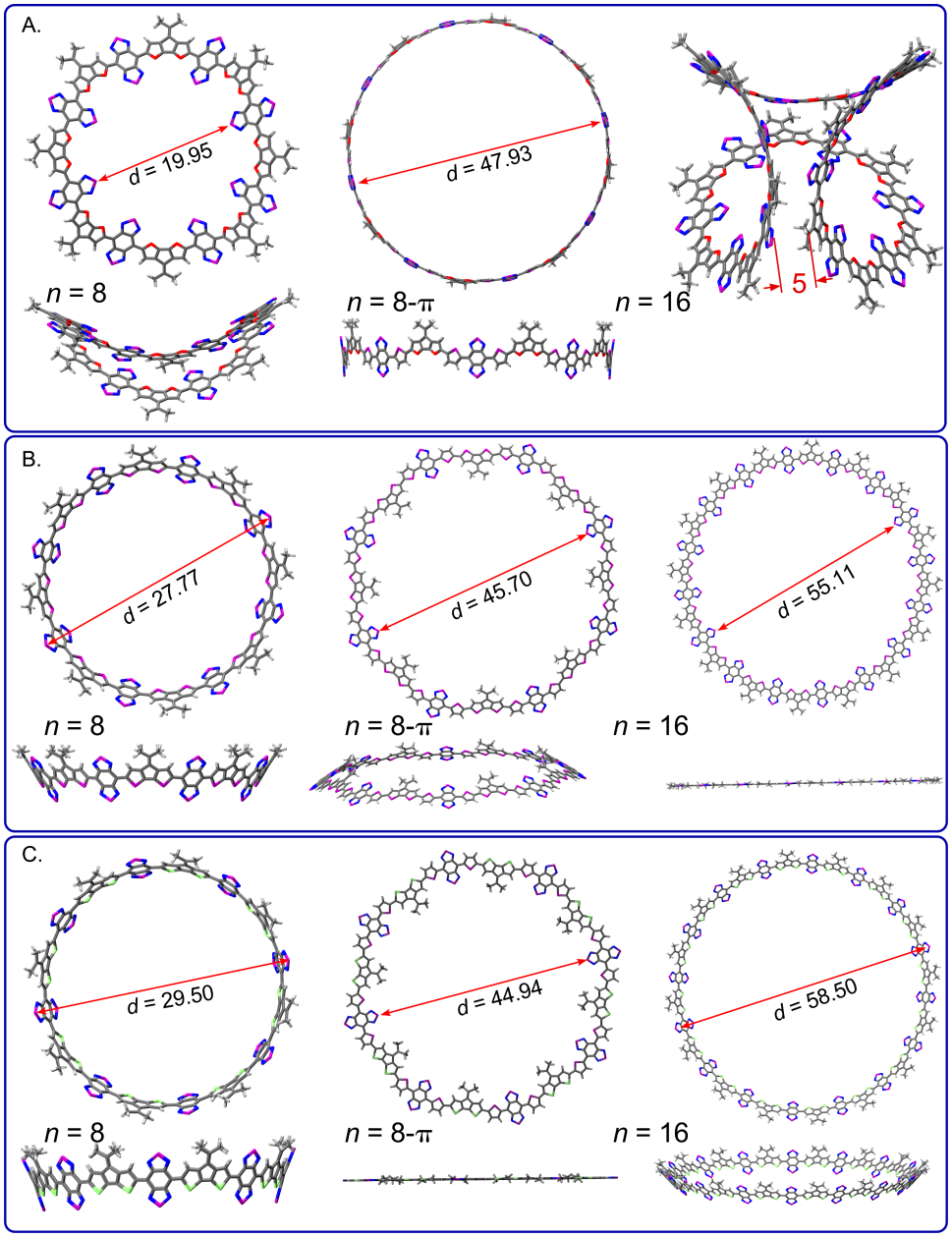

Figure 2: Optimized configurations of CPDF-, CPDT-, and CPDS-BBT macromolecules along their π-spacer derivatives. Geometries shown here: (A) CPDF-BBT, (B) CPDT-BBT, and (C) CPDS-BBT polymer. Calculated distances are in Å.

The CPDT-BBT ($n = 16$) has a planar geometry, with all the dihedral angles close to 180°. This type of planar geometry can elongate the π-conjugation length which improves the π-electron delocalization along the backbone, and reduce the reorganization energy.[38] The CPDS-BBT macromolecule ($n = 16$) also forms a bowl-shaped geometry with the largest

hoop size (58.50 Å) among the macromolecules studied here. Although the observed cavity size is comparable with ethylene substitute oligothiophenes,[39] however, to date, there is no evidence of such large cavity size in D−A organic macromolecules. Also, increasing the ring numbers from $n = 8$ to 16 reduces the distortion along CPDT-BBT and CPDS-BBT backbones, whereas the smallest CPPs are reported to be more planer than the larger ones.[40] The π-spacer substituted ($n = 8 - \pi$) CPDF-BBT is highly rigid and circular, CPDT-BBT is crown-shaped and nonplanar, and CPDS-BBT is completely coplanar. Also, the hoop size for $n = 8 - \pi$ is just the opposite of $n = 8$ due to the more circular nature of the π-spacer substituted CPDF-BBT. The substitution of π-spacer does not improve the dihedral angles of CPDF-BBT from $n = 8$; however, in the case of CPDT-BBT and CPDS-BBT, π-spacer substitution improves the dihedral angles from 175° to 180°. Planar geometry of these macromolecules are obtained probably due to intramolecular non-covalent interactions between heteroatoms of donor and acceptor (O···N, S···N, and Se···N) and hydrogen-bonding interactions, interlocking the two adjacent D and A segments.[41]

We have analyzed the bond lengths to assess the degree of π-conjugation (Fig. S1-S6). The connecting bonds between a donor and adjacent acceptor unit is 1.39 Å with $n = 8$ and 16 repeat units, and 1.42 Å for $n = 8 - \pi$. These bonds are smaller than a C–C single bond (1.45 Å) but larger than a typical double bond (1.35 Å).[21] The mixed single and double bond characteristics of these macromolecules indicate a high degree of π-conjugation throughout the whole π framework, which eventually increases the charge transfer through these macromolecules. The connecting bonds are smallest in the case of CPDF-BBT (Fig. S1 and S2), indicating higher quinoidal character in this molecule. Also, the π-spacer substituted molecules have a larger linker bond (1.41-1.42 Å) than the unsubstituted macromolecules (1.39 Å), indicating a reduction of the AFM coupling between the frontier MOs in the former macromolecules. The bond lengths for the donor and acceptor indicate two distinct bonding patterns for the macromolecules with and without thiophene π-spacer. For $n = 8$ and 16 repeat units, the donor units have alternating single (1.43-1.44 Å) and double bond (1.37-

1.38 Å) characters, indicating a highly quinoidal π-conjugated backbone. The six-member ring in the BBT acceptor unit has bond lengths close to a single bond (1.45 Å), and the C=N bonds in the thiadiazole ring largely shortened. The increased bond length indicates an antiaromatic character in the BBT core with increased aromaticity in the thiadiazole rings. Therefore, a large bond length alternation of these molecules ($n = 8$ and 16) display a closed-shell form in the ground-state.

Interestingly, in the case of the π-spacer macromolecules, bond length alternation has decreased significantly. Nearly equal bonds indicate regaining aromaticity of the heteroatom-containing five-member rings of the donor; although, the quinoidal character exists in the π-spacer and BBT acceptor core. The thiadiazole rings of the BBT still have equal C=N bonds, indicating larger aromaticity on these units. It is clear from the calculated bond lengths on each repeat unit that, two more additional aromatic sextet rings are obtained in each donor along with two thiadiazole rings on the BBT acceptor. Therefore, the aromatic stabilization energy of the π-spacer derivatives has increased to an extent to break a double bond, promoting open-shell character in these macrocycles.

Energetic difference ($\triangle E$) between the ground singlet (S_0) and higher energy states

The ΔE of the polymers with other computed electronic properties provided in Table 1 as a function of the chain length, and an energy diagram of the ground and higher electronic states for the open-shell molecules is shown in Fig. S7. The calculated ΔE_{ST} compares well with the reported values of Saika *et al.*[42] Interestingly, doubling the number of units from $n = 8$ to 16 does not significantly reduce the energy gap between the ground singlet and triplet state (ΔE_{ST}) for the closed-shell macromolecules, a behavior opposite to that observed in linear D−A polymeric systems.[3] The smallest ΔE_{ST} (0.537 eV) in closed-shell systems obtained for CPDT-BBT with $n = 16$, probably due to a more planar geometry

Table 1: Calculated electronic properties for the CPDF-, CPDT-, and CPDS-BBT macromolecules as a function repeating units. The computed energy gap between singlet-triplet (ΔE_{ST}), singlet-quintet (ΔE_{SQT}), singlet-septet (ΔE_{SSP}), and singlet-nonet (ΔE_{SNT}) states, HOMO and LUMO energy values with energetic difference between HOMO-LUMO (E_g). All energy values are in eV.

Polymer	n	ΔE_{ST}	ΔE_{SQT}	ΔE_{SSP}	ΔE_{SNT}	HOMO	LUMO	E_g
	8	0.545	-	-	-	-4.24	-3.01	1.23
CPDF-BBT	8-π	0.636	0.362	1.000	0.928	-4.25	-3.30	0.95
	16	0.545	-	-	-	-4.10	-2.96	1.14
	8	0.563	-	-	-	-4.52	-3.24	1.28
CPDT-BBT	8-π	0.659	0.439	0.675	0.913	-4.39	-3.42	0.97
	16	0.537	-	-	-	-4.47	-3.25	1.22
	8	0.639	-	-	-	-4.62	-3.22	1.40
CPDS-BBT	8-π	0.649	0.367	1.036	0.971	-4.38	-3.43	0.95
	16	0.618	-	-	-	-4.58	-3.23	1.35

of the macrocycle. The calculated ΔE_{ST} gap for the open-shell systems increased from the closed-shell macromolecules, which is probably due to the increased electron-electron repulsions arising from a large number of unpaired electrons within the molecular backbone. We also optimized the structures for quintet, septet, and nonet state for the open-shell molecules with π-spacer. A significant reduction in ΔE_{SQT} (singlet-quintet) gap is observed compared to ΔE_{ST} due to increased separation of the unpaired spins from each other in the polymer backbone (Fig. S10, S16, S22, S28-S30). The smallest ΔE_{SQT} calculated for CPDF-BBT polymer due to a larger cavity size (Fig. 2A) than the other two macrocycles, which facilitates larger separation between the unpaired electrons, therefore, decreasing Coulomb repulsion. Also, a dramatic increase in the ΔE_{SPT} (singlet-septet) and ΔE_{SNT} (singlet-nonet) is observed due to increased electron-electron repulsion in these macromolecules which originates from the increased unpaired electron density in the small region. Furthermore, the calculated ΔE_{SQT} gap is much lower than the singlet closed-shell (SCS) and ΔE_{ST} (Fig. S7), indicating the contribution of high tetraradical character in the singlet ground-state.

Molecular orbitals (MOs) and HOMO-LUMO (E_g) energy gap

Molecular orbitals of the macromolecules show that the highest occupied MO (HOMO) and the lowest unoccupied MO (LUMO) are delocalized along the backbone of the whole macromolecule (Fig. S7-S21), indicating uniform charge transfer, which is predicted by the density difference between the ground to the first singlet excited-state ($\Delta\rho = S_1 - S_0$). For the closed-shell macromolecules, both the thiadiazole rings of the BBT acceptor units are charge deficient, and the residual charges delocalized along the π-conjugation path. However, the open-shell macromolecules show clear charge transfer from the donor to the acceptor moieties. The singly occupied MO (SOMO) of triplet state for $n = 8$ and 16 is more localized than SOMO-1, whereas the two unpaired electrons completely delocalized in the $n = 8$-π macromolecule. Spin density distribution of the triplet state indicates the accumulation of the two unpaired electrons in a small region, which increases the spin-spin repulsions. Therefore, this increases the singlet-triplet energy gaps for $n = 8$ and 16. The spin density of the singlet open-shell molecules is well delocalized along the backbone (Fig. S9, S15, S21), indicating higher thermodynamic stability of these macromolecules in their neutral form. The SOMOs of the higher energy states (i.e., quintet, septet, and nonet) are segregated and localized in different segments of the D−A macromolecules.

Due to the symmetric structure of all the macrocycles, higher energy orbitals are found to be degenerate (Fig. 3, S26-S27). This orbital degeneracy facilitates developing polyradical character, which is extended to hexadecaradical. A similar degeneracy is observed in all macromolecules, except for CPDF-BBT ($n = 16$), where no degeneracy exists in the MOs (Fig. S26). This is due to a zigzag conformation of the macromolecule. For the $n = 8$ repeat units, the both HOMO and LUMO energies are lowered as we go from CPDF- to CPDT- to CPDS-BBT (Table 1). The lowering of HOMO energy value is significant (0.38 eV) for CPDS-BBT than CPDT-BBT from CPDF-BBT polymer. The E_g values follow the

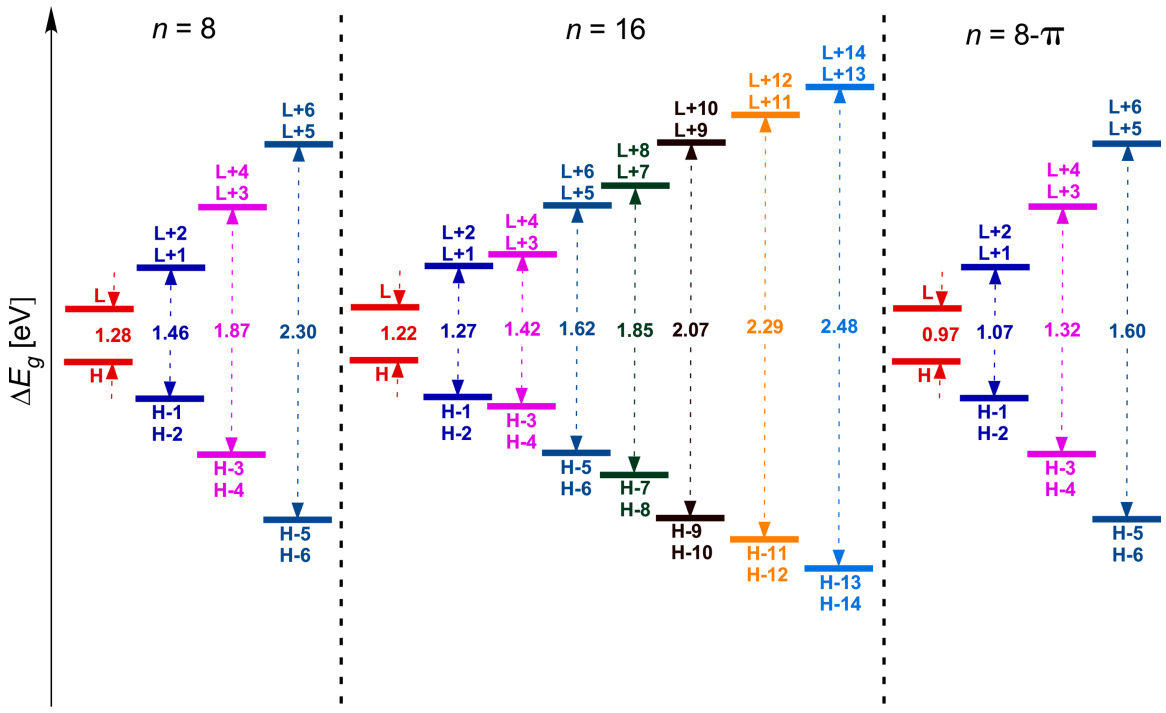

Figure 3: Energy diagram of the frontier and higher degenerate MOs for CPDT-BBT macromolecules obtained as a function of chain length. For $n = 8$ and $n = 8$-π, the orbital degeneracy continues until H-5 (L+5) and H-6 (L+6), however, in case of $n = 16$, it is extended up to H-13 (L+13) and H-14 (L+14). The HOMO-LUMO gaps continues to decrease as we added more repeat units to the backbone, smallest values are obtained in the open-shell systems. Here, H = HOMO, and L = LUMO.

following rank order: CPDF-BBT < CPDT-BBT < CPDS-BBT. Increasing the number of repeat units from $n = 8$ to 16 increases the HOMO energy levels for all macromolecules. A similar trend in the E_g is observed for both $n = 8$ and 16 repeat units, which is opposite to that reported for linear polymers, where larger atomic substitution in acceptor unit reduced the energy gap.[43] In the case of the π-spacer derivatives, the LUMO energies decreased significantly from $n = 8$ and 16 repeat units, and an increase in the HOMO energy is observed for CBDT-BBT and CPDS-BBT oligomers; therefore, the calculated E_g decreased significantly. Both CPDF-BBT and CPDS-BBT have the same E_g values (0.95 eV), slightly different from the CPDT-BBT molecule. To the best of our knowledge, this is the lowest HOMO-LUMO energy gap of any D−A cyclic macromolecules reported. Comparing the E_g values of the closed-shell ($n = 8$ and 16) and open-shell macromolecules, significant reduction

Table 2: Calculated polyradical character of the CPDF-, CPDT-, and CPDS-BBT with π-spacers (n = 8-π). The radical characters reported as the occupation numbers of the lowest unoccupied natural orbitals (LUNO+i).

Polymer	y_0	y_1	y_2	y_3	y_4	y_5	y_6	y_7
CPDF-BBT	0.992	0.517	0.517	0.268	0.268	0.170	0.170	0.144
CPDT-BBT	0.916	0.525	0.525	0.279	0.279	0.179	0.179	0.153
CPDS-BBT	0.937	0.516	0.516	0.267	0.267	0.167	0.167	0.140

in E_g is observed for the latter one. Previous studies on macromolecules have shown that a reduction in the number of repeat unit or small loop size fine-tunes the HOMO-LUMO energy gaps.[40]

Polyradical character (y_i)

The y_i values for the macromolecules (n = 8-π) presented in Table 2. It is reported that a moderate AFM coupling between the unpaired electrons leads to polyradical character in macrocyclic molecules; however, a very strong AFM coupling diminishes polyradical character.[16,19] The macrocycles with $n = 8$ and 16 repeat units do not have an open-shell character, which is due to very strong AFM coupling between the unpaired electrons in the frontier MOs, as evidenced by reduced linker bonds between the donor and acceptor units. However, insertion of the thiophene π-spacer leads tp polyradical character in the molecules. All the macromolecules (n = 8-π) have near pure-open shell diradical character, indicated by y_0 values, which is close to 1. The CPDF-BBT has higher y_0 than the other two macromolecules, lowest value is obtained for CPDT-BBT. This is due to a larger cavity size of the CPDF-BBT macrocycle compared to the other two macromolecules, which increases the distance between the unpaired electrons, consequently, decreasing the electron-electron coupling. This is also reflected by a lower singlet-triplet (ΔE_{ST}) energy gap for CPDF-BBT than CPDT-BBT and CPDS-BBT macromolecules. All the macromolecules have high tetraradical (y_1) and hexaradical (y_2) characters, moderate octaradical (y_3) and decaradical (y_4) characters and low dodeca- (y_5), tetradeca- (y_6), and hexadecaradical (y_7) characters. Although, the calcu-

lated polyradical characters are comparable with the reported values in the literature,[14,19,44] to date, radical characters beyond decaradical is not reported for macrocycles. Interestingly, polyradical character larger than y_0 obtained as pairs, except for hexadecaradical (y_7). This is due to the degeneracy between LUMO+1 and LUMO+2 (for y_1 and y_2), LUMO+3 and LUMO+4 (for y_3 and y_4) and between LUMO+5 and LUMO+6 (for y_5 and y_6) (Fig. 3, S26-S27). The degeneracy lifted after LUMO+6 and higher degenerate orbitals are not energetically accessible. Therefore, the polyradical character developed up to y_7. We believe that, more degenerate orbitals would increase the polyradical character above hexadecaradical, however, DFT calculation is intractable for larger chain lengths with the π-spacer (n = 16-π). Except the diradical character, higher radical characters of CPDT-BBT are consistently larger than CPDF-BBT and CPDS-BBT macromolecules. This is probably due to low energy difference between the degenerate occupied and unoccupied MOs (Fig. 3).

Aromaticity of the D−A macrocycles

An interesting feature of the π-conjugated macrocycles is that they display global (anti)aromaticity. Here, we used the nucleus-independent chemical shift (NICS),[45] anisotropy of the induced current density (AICD),[46] and 2D-iso-chemical shielding surface (2D-ICSS)[47] methods to analyze the global (anti)aromaticity of the macrocycles. The CPDF-, CPDT-, and CPDS-BBT macromolecules with n = 8 and 16 repeat units have a NICS(0) value close to 0 (Table S1, Fig. S1, S3, S5), indicating global nonaromaticity, with local aromaticity on the individual rings.[48] Even though, the macrocycles with n = 8 and 16 repeat units have 96π and 192π (128π and 256π through the hypervalent sulfur of BBT acceptor) ($4N\pi$) electrons conjugated pathway (Fig. 1D), respectively, due to the very high quinoidal character of these macrocycles, aromaticity is localized on the individual rings along the backbone. This localization of aromaticity can also be observed from the AICD plots and 2D-ICSS maps (Fig. S31, S33, S35–S53), where the ring current is localized on the individual rings and a significant

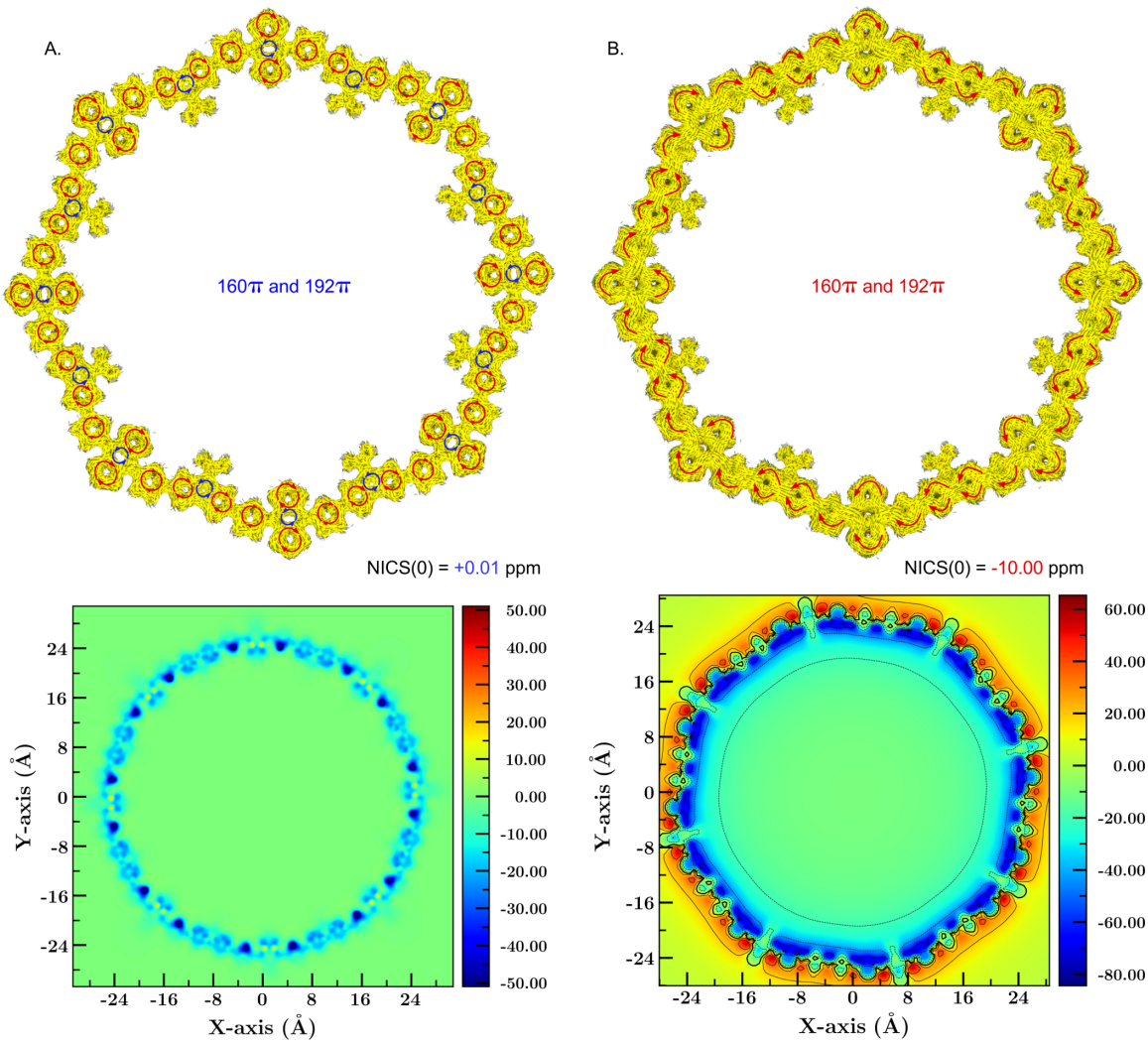

Figure 4: AICD plots (top) and 2D-ICSS (bottom) maps for CPDT-BBT in the (A) singlet and (B) triplet states, respectively, at n = 8-π. The blue and red arrows along the molecular backbone indicates counter-clockwise (paratropic) and clockwise (diatropic) ring current flow, respectively. The direction of the applied magnetic field is perpendicular to the ring plane and points out through the paper. AICD plots are generated with an isovalue = 0.025 au.

magnetic shielding (negative 2D-ICSS) is observed along the conjugated backbone.

Although the NICS(0) values for the open-shell CPDF-, CPDT-, and CPDS-BBT macromolecules (n = 8-π) in the singlet ground-state is close to 0 (Fig. 4, S2, S4, S6), the calculated NICS(0) in their triplet states are negative (-9.82 ppm, -10.00 ppm, and -10.30 ppm for CPDF-, CPDT-, and CPDS-BBT, respectively) (Table S2, Fig. S2, S4, S6). Therefore, the lowest triplet state of the CPDF-, CPDT-, and CPDS-BBT macromolecules with n =

8-π shows a global aromatic character with $4N\pi$ electrons, a manifestation of Baird's rule.[37] This phenomenon is reported for a highly conjugated bis-rhodium hexaphyrins,[49] or in a AWA super-ring structure,[19] but not observed in D−A macromolecules. The AICD plots for the triplet state unambiguously indicate a unidirectional clockwise (diatropic) current flow along the 160π and 192π ($4N\pi$) electrons conjugated pathway, respectively, which indicates a global aromatic character. The 2D-ICSS maps (Fig. 4B, S32B, S34B) show the inside region of the macrocycles is magnetically shielded (negative 2D-ICSS value), further supporting global aromaticity in the triplet state. The higher energy (quintet, septet, and nonet) states have very small NICS(0) values (Table S2), indicating global nonaromaticity.

NICS(0) calculations of CPDF-BBT, CPDT-BBT and CPDS-BBT (n = 8) on the individual rings along the backbone indicate the heteroatom-containing five-member rings on the donor units have small aromaticity (NICS(0) $\approx$ -4.00 to -4.70 ppm), while the aromaticity has increased substantially (NICS(0) $\approx$ -7.00 to -7.75 ppm) in case of the π-spacer derivative (n = 8-π) (Fig. S3–S6). The thiadiazole rings of the BBT acceptor units show increased NICS(0) values in case of the π-spacer derivatives than the macromolecules without π-spacer (n = 8 amd 16). Therefore, it is evident that the heteroatom-containing five-member rings in the donor unit of CPDF-BBT, CPDT-BBT and CPDS-BBT (n = 8-π) have regained aromatic character along with the thiadiazole rings in the BBT acceptor unit. The aromaticity of the donor units also consistent with the calculated bond lengths of the macromolecules, where reduced bond length alternations on the donor indicated the aromatic character of the heteroatom-containing five-member rings. All the thiophene π-spacers have negative NICS(0) values. Therefore, the aromatic stabilization energy has increased in π-spacer derivatives than the unsubstituted systems, facilitating double bond-breaking along the π-conjugated backbone. These results indicate the polyradical character of the π-spacer derivatives, but not on n = 8 and 16 repeating units.

Optical properties

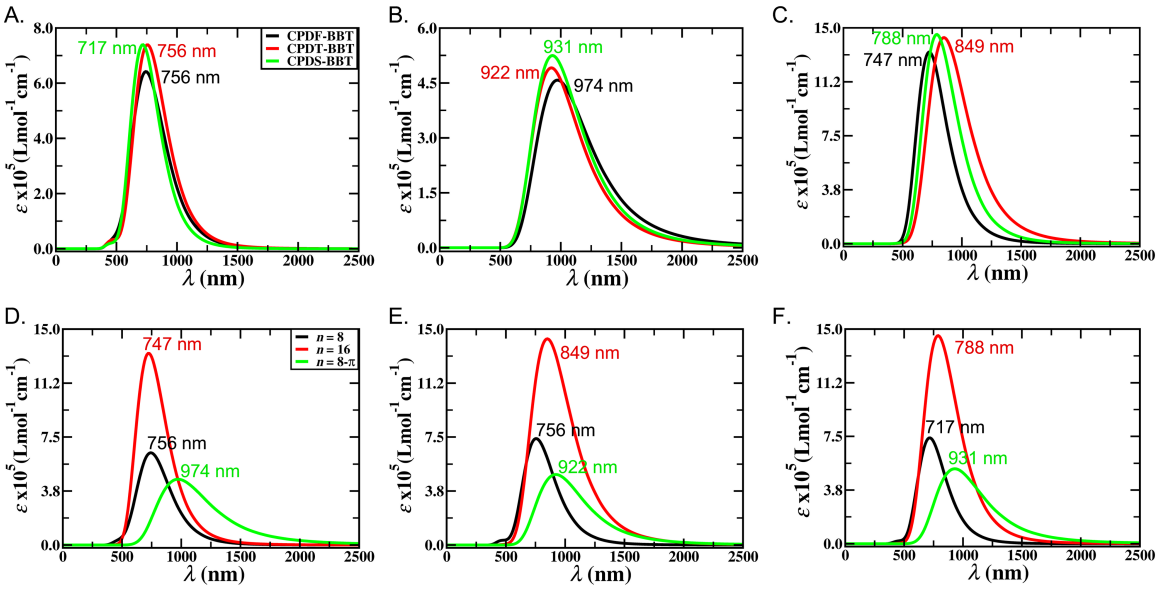

Figure 5: Absorption spectra of the CPDF-, CPDT-, and CPDS-BBT macromolecules. (A) $n = 8$, (B) $n = 8$-π, (C) $n = 16$, (D) CPDF-BBT, (E) CPDT-BBT, and (F) CPDS-BBT. Calculations are performed with PCM/TD-(U)CAM-B3LYP on the optimized ground-state geometry in the presence of chloroform.

The optical properties of the macromolecules are explored with the time-dependent density functional theory (TDDFT). It is evident from the calculated spectra that, the absorption occurs in the near-infrared (NIR) region (Fig. 5). Comparing the absorption spectra of CPDF-, CPDT-, and CPDS-BBT macromolecules for $n = 8$ repeat unit, the maximum absorption occurs within 717-756 nm, with CPDF-BBT and CPDT-BBT having similar absorption maximum at 756 nm. For the CPPs, the maximum absorption reported only around 340 nm,[50] making CPPs less attractive in the optoelectronic devices, whereas in this case, absorption is extended into the NIR region, which is not reported in case of cyclic D−A macromolecules.[26,28,31] A small shoulder is present for both CPDT-BBT and CPDS-BBT macrocycles only with $n = 8$ repeat units. In case of CPDT-BBT, the shoulder corresponds to a double-degenerate absorption at 462 nm, with orbital transition occurring from HOMO to LUMO+1 and LUMO+2 ($f = 0.3476$). Similar orbital transitions involved for CPDS-BBT also, with double-degenerate absorption at 447 nm ($f = 0.1861$). The π-conjugation length

Table 3: Tabulated optical properties for CPDF-, CPDT-, and CPDS-BBT macromolecules provided as a function of oligomer length. The calculated excitations from the ground-state, excitation energies (E_g), the wavelength of the excitations (λ), oscillator strengths of the excitation (f), MOs involved in the transitions, and percent contribution of the individual transitions. The calculations performed at PCM/(U)CAM-B3LYP level and chloroform used as an implicit solvent.

Polymer	n	Excitations	E_g (eV)	λ (nm)	f	Orbital contributions	
CPDF-BBT	8	$S_0 \rightarrow S_1$	1.44	862.24	0.00	H→L (37%)	
		$S_0 \rightarrow S_2$	1.64	757.29	7.25	H→L+1 (35%)	
		$S_0 \rightarrow S_3$	1.64	756.22	7.26	H→L+2 (35%)	
		$S_0 \rightarrow S_5$	1.97	628.53	2.42	H→L+4 (30%)	
	16	$S_0 \rightarrow S_1$	1.41	878.03	0.01	H-1→L+1 (13%)	
		$S_0 \rightarrow S_2$	1.45	851.59	0.98	H-2→L (19%)	
		$S_0 \rightarrow S_3$	1.46	849.45	1.05	H→L+1 (13%)	
		$S_0 \rightarrow S_5$	1.66	747.24	14.96	H→L+3 (16%)	
		$S_0 \rightarrow S_6$	1.77	698.62	8.54	H→L+6 (14%)	
		$S_0 \rightarrow S_7$	1.77	698.62	8.54	H→L+6 (14%)	
	8-π	$S_0 \rightarrow S_1$	1.22	1015.70	0.00	H(α)→L(α) (16%)	H(β)→L(β) (16%)
		$S_0 \rightarrow S_2$	1.27	974.03	5.61	H(α)→L(α)+1 (16%)	H(β)-2→L(β) (14%)
		$S_0 \rightarrow S_3$	1.27	974.03	5.61	H(α)→L(α)+2 (16%)	H(β)-1→L(β) (14%)
CPDT-BBT	8	$S_0 \rightarrow S_1$	1.45	853.95	0.00	H→L (34%)	
		$S_0 \rightarrow S_2$	1.64	755.80	9.13	H→L+1 (34%)	
		$S_0 \rightarrow S_3$	1.64	755.80	9.13	H→L+2 (34%)	
	16	$S_0 \rightarrow S_1$	1.40	887.48	0.00	H→L (18%)	
		$S_0 \rightarrow S_2$	1.46	849.22	17.69	H→L+1 (13%)	
		$S_0 \rightarrow S_3$	1.46	849.22	17.69	H→L+2(13%)	
	8-π	$S_0 \rightarrow S_1$	1.30	956.34	0.00	H(α)→L(α) (16%)	H(β)→L(β) (16%)
		$S_0 \rightarrow S_2$	1.34	921.79	6.03	H(α)→L(α)+1 (12%)	H(β)→L(β)+2 (16%)
		$S_0 \rightarrow S_3$	1.34	921.79	6.03	H(α)→L(α)+2 (13%)	H(β)→L(β)+1 (16%)
CPDS-BBT	8	$S_0 \rightarrow S_1$	1.56	794.60	0.00	H→L (31%)	
		$S_0 \rightarrow S_2$	1.73	716.95	9.13	H→L+1 (31%)	
		$S_0 \rightarrow S_3$	1.73	716.95	9.13	H→L+2 (31%)	
	16	$S_0 \rightarrow S_1$	1.52	817.63	0.00	H→L (16%)	
		$S_0 \rightarrow S_2$	1.57	788.39	17.95	H→L+1 (16%)	
		$S_0 \rightarrow S_3$	1.57	788.39	17.95	H→L+2 (16%)	
	8-π	$S_0 \rightarrow S_1$	1.28	967.65	0.00	H(α)→L(α) (16%)	H(β)→L(β) (16%)
		$S_0 \rightarrow S_2$	1.33	930.79	6.45	H(α)→L(α)+1 (15%)	H(β)-2→L(β) (14%)
		$S_0 \rightarrow S_3$	1.33	930.79	6.45	H(α)→L(α)+2 (15%)	H(β)-2→L(β) (14%)

H = HOMO; L = LUMO; α = spin-up; β = spin-down

is elongated in $n = 16$ repeat units, therefore, the excitation coefficients increased by almost three times than $n = 8$ and $n = 8$-π for all macrocycles. The maximum absorption occurs

within 747-849 nm, with CPDF-BBT absorption blue-shifted by 9 nm, and CPDT-BBT and CPDS-BBT spectra is red-shifted by 93 nm and 71 nm from $n = 8$, respectively. The blue-shift in CPDF-BBT spectra occurs due to its twisted configuration and weaker π-conjugation along the backbone (Fig. 2A), although a reduction in the HOMO-LUMO gap observed from $n = 8$ to 16. Therefore, increasing the chain lengths facilitates red-shifting the absorption spectra in these macromolecules. In case of the CPPs nano hoops, the absorption maxima is found to be size-independent.[50] However, clearly, size-dependent absorption found in this case.[39] Also, due to the narrowing of the HOMO-LUMO gap, a large red-shift observed for all π-spacer derivative macromolecules, now the absorption maximum varies within 922-974 nm. Here, the absorption spectra red-shifted for CPDF-, CPDT-, and CPDS-BBT by 218 nm, 166 nm, and 214 nm from $n = 8$, respectively and by 227 nm, 73 nm , and 143 nm from $n = 16$, respectively. Furthermore, the absorption is broadened up to 2500 nm, showing extended absorption in the whole near-infrared (NIR) region. This extended absorption is due to the antiaromatic nature of the ground-state and attributed to the forbidden transitions in the macrocycles.[19]

All the optical excitations from ground to the first singlet excited-state ($S_0 \rightarrow S_1$) are optically forbidden (Table 3), indicated by zero oscillator strengths ($f = 0.0$) for the transition. Similar findings reported for cyclic CPPs and other macrocycle.[40] This forbidden transition included electronic excitation from HOMO→LUMO. This indicates the high symmetry of these molecular orbitals involved in the transition. Interestingly, all the allowed transitions obtained as doubly-degenerate both for closed- and open-shell macromolecules. This is due to the degenerate MOs for all the macromolecules (Fig. 3, S26-S27). In all cases, the allowed transitions involved excitation from the ground to the second and third excited-state ($S_0 \rightarrow S_2$ and $S_0 \rightarrow S_3$), except for CPDF-BBT ($n = 16$), where all the excitations from lower energy states are allowed, having S_6 and S_7 excited-states as doubly-degenerate. For the closed-shell macromolecules, the allowed transitions assigned as HOMO to LUMO+1, HOMO to LUMO+2, and HOMO to LUMO+4. For CPDF-BBT ($n = 16$), the maximum

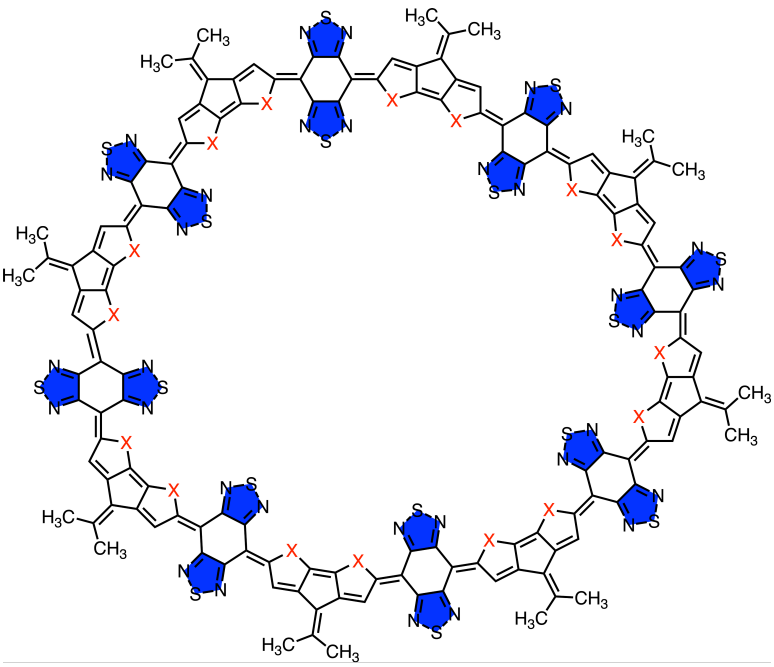

Figure 6: Closed-shell resonance structure of the CPDF-(X = O), CPDT-(X = S), and CPDS-BBT (X = Se) macromolecules with $n = 8$ repeat units. The aromatic thiadiazole units are shown in blue.

oscillator strength ($f = 14.96$) observed in HOMO to LUMO+3 transition, with degenerate excitation assigned to HOMO to LUMO+5 and HOMO to LUMO+6. In the case of the open-shell structure, the HOMO to LUMO transitions is still forbidden, with allowed transition assigned to HOMO-2 to LUMO, HOMO-1 to LUMO, and the other allowed transition obtained similar to the closed-shell system.

Origin of radical characters

The process of developing polyradical character in a molecule involves the generation of multiple unpaired electrons by breaking carbon-carbon double bonds within the π-framework. The driving force required to break a double bond to create a diradical would be much smaller than breaking multiple double bonds to generate polyradical character. This "driving force" ascribed to the recovery of aromatic stabilization energy of the quinoidal units in the backbone, more recovery of the aromatic rings would increase this driving force to create

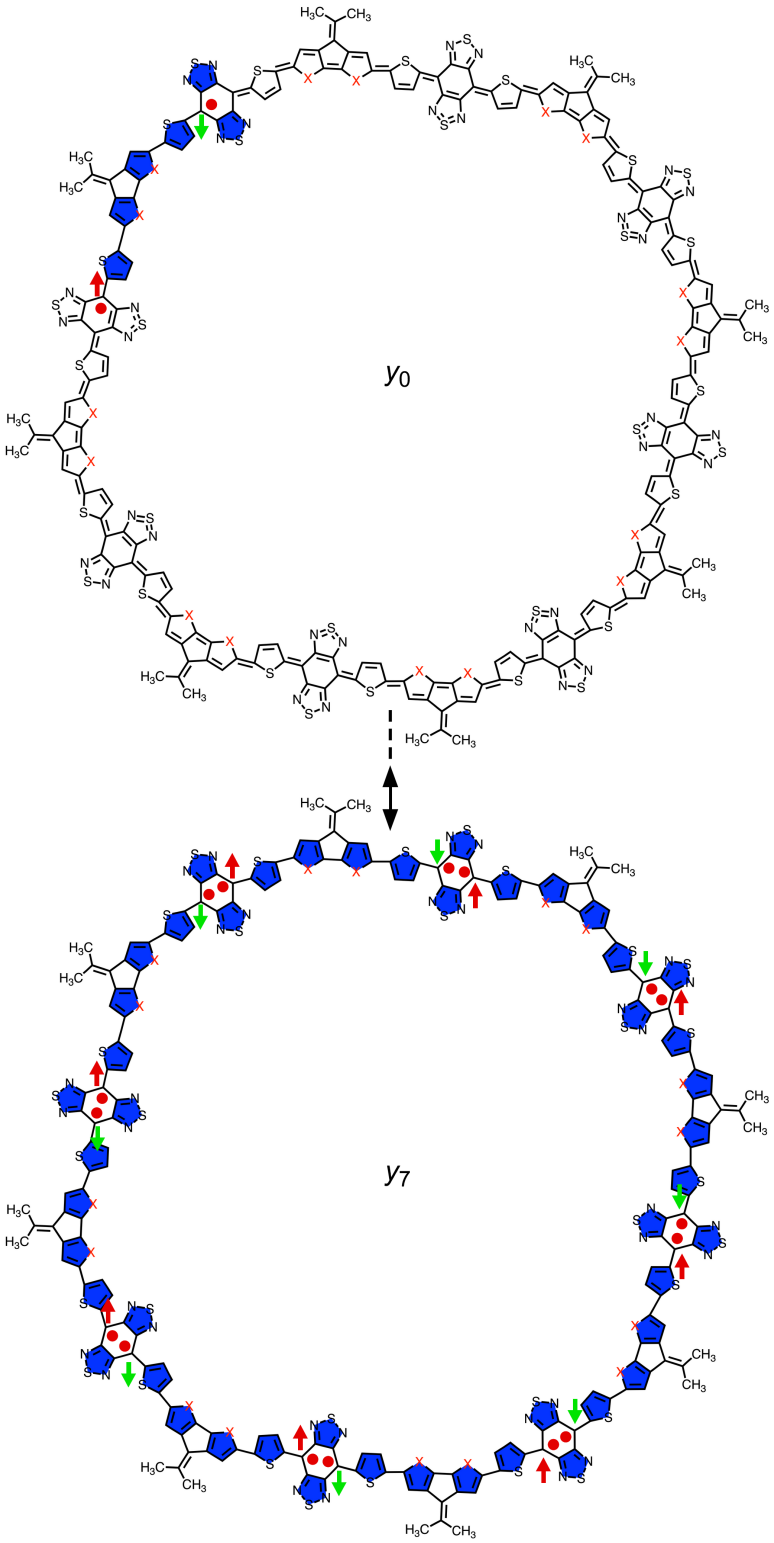

Figure 7: Resonance structures of the CPDF-(X = O), CPDT-(X = S), and CPDS-BBT (X = Se) macromolecules with n = 8-π repeat units. Gradual development of radical characters from diradical to hexadecaradical is achieved by more aromatic sextet rings (highlighted in blue) in the π-framework. Red and green arrows indicate up- and down-spins, respectively.

diradical and polyradical character.[14] The BBT acceptor can show diradical character by the recovery of additional thiadiazole rings, therefore, BBT has long recognized as an intrinsic open-shell unit.[35,51] Although, two aromatic sextet thiadiazole units recovered in each BBT units in the backbone (Fig. 6), the macrocycles with $n = 8$ repeat units does not show any radical characters ($y_i = 0$). The strong AFM coupling between the spins prohibit developing unpaired electrons in the π-framework.[19] Therefore, all the macromolecules with $n = 8$ and 16 repeat units characterized as a highly quinoidal closed-shell oligomer, and in these cases, the BBT acceptor did not impart any radical characters in these macrocycles. On the other hand, by inserting π-spacer in the polymer backbone, two additional aromatic sextet rings in the donor regained aromatic stabilization energy along with the two thiadiazole units in each BBT acceptor (Fig. 7, S54-S57). Therefore, sufficient stabilization energy obtained to transform from closed-shell to the open-shell form. Here, one additional double-bond has broken to have diradical (2 unpaired electrons) to tetraradical (4 unpaired electrons) and reaching up to hexadecaradical (16 unpaired electrons) characters in these macromolecules (Fig. S54-S57). The degenerate MOs fueled the generation of polyradical character extended up to hexadecaradical. The $n = 8$ and 16 have enough degenerate MOs (Fig. 3, S26-S27), but the driving force to overcome the π-bond covalency is not enough to produce polyradical character. Therefore, the macromolecules with $n = 8$ and $n = 16$ repeat units does not show any radical characters.

DISCUSSION

In conclusion, for the first time, D−A macromolecules are designed and analyzed with computational investigations, which show near pure diradical character and moderate-to-high polyradical character. The closed-shell molecules show a similar singlet-triplet and HOMO-LUMO energy gap, and global nonaromatic character. However, open-shell molecules have higher singlet-triplet and significantly reduced HOMO-LUMO energy gaps. While the macro-

molecules without π-spacer have significant bond length alternations, indicating high quinoidal character, the π substituted derivatives reduce bond length alternations, indicating regain of aromatic stabilization energy in the donor units. Therefore, the π-spacer derivatives develop near pure diradical and moderate-to-high polyradical characters, which extended up to hexadecaradical character. Also, while the singlet ground-state shows a global antiaromatic character according to H*ü*ckel's rule ($4N\pi$ electrons), the lowest triplet state of the open-shell molecules indicates global aromatic character following Baird's rule, which is not observed in the D−A type macromolecules. Furthermore, the TDDFT calculations indicate NIR absorption with absorption spectra broadening to 2500 nm and a significant red-shift in the absorption maxima observed from closed-shell to open-shell macromolecules. Our work shows that these molecules can be potential synthetic targets for optoelectronic devices, in particular, as NIR sensors and non-linear optics (NLO) applications.

Methods

Computational details

All the calculations are performed with Gaussian 16 software package.[52] Molecular geometries for the singlet and higher electronic states of the model oligomers (n = 8, 16, and 8-π) are optimized in the gas phase using hybrid density functional, B3LYP.[53] For the *Se* atom, LANL2DZdp basis set is used along with associated effective core potentials,[54] with 6-31G(*d, p*)[55] basis set for other the atoms. All parameters for geometry optimizations set to defaults. For the oligomers, geometries considered optimized once the RMS forces on all atoms converged to zero.[56] A single-reference wave function cannot determine the electronic structure of open-shell molecules.[4] Multi-reference configuration schemes are computationally very demanding; therefore, a broken-symmetry (BS)[57] wave function used to characterize the open-shell singlet state. The triplet and higher spin-states optimized with an unrestricted wave function.

A molecule with two unpaired electrons localized at two degenerate or nearly degenerate non-bonding molecular orbitals (NBMOs) is a diradical.[4] The electronic properties of an open-shell molecule is best defined by a quantitative multi-radical (or polyradical) index, y_i (i = 0-7), which is an indication of the degree of localization of pair of electrons at different sites. A high value of y_i indicates a high degree of electron correlation, i.e., doubly-excited electronic configuration has a higher weight in the ground-state electronic wave function.[6] Theoretically, y_i is defined as the occupation number of the lowest unoccupied natural orbitals (LUNO+i).[58] In case of a closed-shell molecule, the orbital occupancy can be either 2 (doubly occupied) or 0 (empty orbital), however, in case of an open-shell molecule, this occupancy varies in between 0 and 2.[6] Therefore, for a closed-shell molecule, the LUNO+i occupancy is 0 and it increases as the molecule start to develop open-shell character, and approaches a value of 1 for a pure open-shell molecule. Therefore, a closed-shell ($y_i = 0$), intermediate ($0 < y_i < 1$), and pure ($y_i = 1$) polyradical molecule can be defined by y_i values.[3] Here, the polyradical (y_i) indexes obtained from population analysis of natural orbitals as the occupation numbers of lowest unoccupied natural orbitals (LUNOs).

NICS is an excellent probe for the magnetic index of aromaticity or antiaromaticity of a molecule. A high negative NICS value indicates molecule as aromatic, a positive NICS value indicates as antiaromatic, and a 0 (zero) value indicates the corresponding molecule as nonaromatic. Nucleus independent chemical shift (NICS(0))[59] is computed by the gauge-independent atomic orbital (GIAO)[60] method on the optimized geometry by single point energy calculation placing a ghost atom at the center of the macromolecules and also on each rings along the conjugated backbone.

NBO6 program package[61] is used to predict the spin location from natural spin densities of the Kohn-Sham MOs. Time-dependent DFT (TDDFT) calculation at the (U)CAM-B3LYP[62] level is used to simulate the lowest 20 singlet excited states with Tamm-Dancoff approximation[63] in the presence of implicit solvent. Integral equation formalism (IEFPCM) of the Polarizable Continuum Model (PCM)[64] is used with chloroform as the implicit solvent.

AICD (anisotropy of the induced current density) plots are generated by method developed by Herges *et al.*[46] and 2D-ICSS (2D-iso-chemical shielding surface) maps generated by the method developed by Klod *et al.*[47]

DATA AVAILABILITY

The data that support the findings of this study are available from the corresponding author (NR) upon reasonable request.

Acknowledgements

This work is supported by the National Science Foundation (NSF) under grant no. OIA-1757220. The DFT calculations performed at the high-performance computing center at Mississippi State University. Also, the Extreme Science and Engineering Discovery Environment (XSEDE) is used, which is supported by NSF grant number ACI-1548562. We acknowledge the Texas Advanced Computing Center (TACC) at The University of Texas at Austin for providing (HPC, Stampede 2 (through XSEDE allocation, TG-CHE140141)) resources that have contributed to the research results reported within this paper.

Competing Interests

The authors declare that they have no competing financial interests.

Author Contributions

MAS conceived the design idea and performed the DFT calculations and analysis with inputs from NR. MAS wrote the first draft of the manuscript. MMH developed codes for generating AICD and 2D-ICSS diagrams. NR supervised the project and revised the manuscript.

Correspondence

Correspondence and requests for materials should be addressed to Neeraj Rai (email: neerajrai@che.msstate.edu).

Supplementary Information

Supplementary information is available for this paper at

Literature Cited

(1) Lewis, S. E. Cycloparaphenylenes and related nanohoops. *Chem. Soc. Rev.* **2015**, *44*, 2221–2304.

(2) Gopalakrishna, T. Y.; Zeng, W.; Lu, X.; Wu, J. From open-shell singlet diradicaloids to polyradicaloids. *ChemComm.* **2018**, *54*, 2186–2199.

(3) London, A. E.; Chen, H.; Sabuj, M.; Tropp, J.; Saghayezhian, M.; Eedugurala, N.; Zhang, B.; Liu, Y.; Gu, X.; Wong, B.; Rai, N.; Azoulay, J. A high-spin ground-state donor-acceptor conjugated polymer. *Sci. Adv.* **2019**, *5*, eaav2336.

(4) Abe, M. Diradicals. *Chem. Rev.* **2013**, *113*, 7011–7088.

(5) Rajca, A. Organic diradicals and polyradicals: from spin coupling to magnetism? *Chem. Rev.* **1994**, *94*, 871–893.

(6) Nakano, M. Open-Shell-Character-Based Molecular Design Principles: Applications to Nonlinear Optics and Singlet Fission. *Chem. Rec.* **2017**, *17*, 27–62.

(7) Mas-Torrent, M.; Crivillers, N.; Mugnaini, V.; Ratera, I.; Rovira, C.; Veciana, J. Organic radicals on surfaces: towards molecular spintronics. *J. Mater. Chem.* **2009**, *19*, 1691–1695.

(8) Wang, K.; Huang, L.; Eedugurala, N.; Zhang, S.; Sabuj, M. A.; Rai, N.; Gu, X.; Azoulay, J. D.; Ng, T. N. Wide Potential Window Supercapacitors Using Open-Shell Donor–Acceptor Conjugated Polymers with Stable N-Doped States. *Adv. Energy Mater.* **2019**, *9*, 1902806.

(9) Dang, D.; Yu, D.; Wang, E. Conjugated Donor–Acceptor Terpolymers Toward High-Efficiency Polymer Solar Cells. *Adv. Mater.* **2019**, *31*, 1807019.

(10) Kanimozhi, C.; Yaacobi-Gross, N.; Chou, K. W.; Amassian, A.; Anthopoulos, T. D.; Patil, S. Diketopyrrolopyrrole–diketopyrrolopyrrole-based conjugated copolymer for high-mobility organic field-effect transistors. *J. Am. Chem. Soc.* **2012**, *134*, 16532–16535.

(11) Yang, Y.; Farley, R. T.; Steckler, T. T.; Eom, S.-H.; Reynolds, J. R.; Schanze, K. S.; Xue, J. Near infrared organic light-emitting devices based on donor-acceptor-donor oligomers. *Appl. Phys. Lett.* **2008**, *93*, 388.

(12) Bronstein, H.; Chen, Z.; Ashraf, R. S.; Zhang, W.; Du, J.; Durrant, J. R.; Shakya Tuladhar, P.; Song, K.; Watkins, S. E.; Geerts, Y. Thieno [3, 2-b] thiophene-diketopyrrolopyrrole-containing polymers for high-performance organic field-effect transistors and organic photovoltaic devices. *J. Am. Chem. Soc.* **2011**, *133*, 3272–3275.

(13) Steckler, T. T.; Zhang, X.; Hwang, J.; Honeyager, R.; Ohira, S.; Zhang, X.-H.; Grant, A.; Ellinger, S.; Odom, S. A.; Sweat, D. A spray-processable, low bandgap, and ambipolar donor- acceptor conjugated polymer. *J. Am. Chem. Soc.* **2009**, *131*, 2824–2826.

(14) Das, S.; Herng, T. S.; Zafra, J. L.; Burrezo, P. M.; Kitano, M.; Ishida, M.; Gopalakrishna, T. Y.; Hu, P.; Osuka, A.; Casado, J. Fully fused quinoidal/aromatic carbazole macrocycles with poly-radical characters. *J. Am. Chem. Soc.* **2016**, *138*, 7782–7790.

(15) Nobusue, S.; Miyoshi, H.; Shimizu, A.; Hisaki, I.; Fukuda, K.; Nakano, M.; Tobe, Y. Tetracyclopenta [def, jkl, pqr, vwx] tetraphenylene: A Potential Tetraradicaloid Hydrocarbon. *Angew. Chem. Int. Ed.* **2015**, *54*, 2090–2094.

(16) Hu, P.; Lee, S.; Herng, T. S.; Aratani, N.; Gonçalves, T. P.; Qi, Q.; Shi, X.; Yamada, H.; Huang, K.-W.; Ding, J. Toward tetraradicaloid: The effect of fusion mode on radical character and chemical reactivity. *J. Am. Chem. Soc.* **2016**, *138*, 1065–1077.

(17) Lu, X.; Lee, S.; Kim, J. O.; Gopalakrishna, T. Y.; Phan, H.; Herng, T. S.; Lim, Z.; Zeng, Z.; Ding, J.; Kim, D. Stable 3, 6-linked fluorenyl radical oligomers with intramolecular antiferromagnetic coupling and polyradical characters. *J. Am. Chem. Soc.* **2016**, *138*, 13048–13058.

(18) Lu, X.; Lee, S.; Hong, Y.; Phan, H.; Gopalakrishna, T. Y.; Herng, T. S.; Tanaka, T.; Sandoval-Salinas, M. E.; Zeng, W.; Ding, J. Fluorenyl based macrocyclic polyradicaloids. *J. Am. Chem. Soc.* **2017**, *139*, 13173–13183.

(19) Liu, C.; Ni, Y.; Lu, X.; Li, G.; Wu, J. Global Aromaticity in Macrocyclic Polyradicaloids: Huckel's Rule or Baird's Rule? *Acc. Chem. Res.* **2019**, *52*, 2309–2321.

(20) Li, G.; Han, Y.; Zou, Y.; Lee, J. J. C.; Ni, Y.; Wu, J. Dearomatization Approach Toward Superbenzoquinone-Based Diradicaloid, Tetraradicaloid, and Hexaradicaloid. *Angew. Chem.* **2019**, *131*, 14457–14464.

(21) Li, Z.; Gopalakrishna, T. Y.; Han, Y.; Gu, Y.; Yuan, L.; Zeng, W.; Casanova, D.; Wu, J. [6] Cyclo-para-phenylmethine: An Analog of Benzene Showing Global Aromaticity and Open-shell Diradical Character. *J. Am. Chem. Soc.* **2019**, *141*, 16266–16270.

(22) Liu, C.; Sandoval-Salinas, M. E.; Hong, Y.; Gopalakrishna, T. Y.; Phan, H.; Aratani, N.; Herng, T. S.; Ding, J.; Yamada, H.; Kim, D. Macrocyclic polyradicaloids with unusual super-ring structure and global aromaticity. *Chem* **2018**, *4*, 1586–1595.

(23) Ball, M.; Nuckolls, C. Stepping into the Light: Conjugated Macrocycles with Donor–Acceptor Motifs. 2015.

(24) Van Raden, J.; Darzi, E.; Zakharov, L.; Jasti, R. Synthesis and characterization of a highly strained donor–acceptor nanohoop. *Org. Biomol. Chem.* **2016**, *14*, 5721–5727.

(25) Yu, Y.; Bian, L.; Zhang, Y.; Liu, Z.; Li, Y.; Zhang, R.; Ju, R.; Yin, C.; Yang, L.; Yi, M. Synthesis of Donor–Acceptor Gridarenes with Tunable Electronic Structures for Synaptic Learning Memristor. *ACS Omega* **2019**, *4*, 5863–5869.

(26) Ball, M.; Zhong, Y.; Fowler, B.; Zhang, B.; Li, P.; Etkin, G.; Paley, D. W.; Decatur, J.; Dalsania, A. K.; Li, H. Macrocyclization in the design of organic n-type electronic materials. *J. Am. Chem. Soc.* **2016**, *138*, 12861–12867.

(27) Ball, M. L.; Zhang, B.; Xu, Q.; Paley, D. W.; Ritter, V. C.; Ng, F.; Steigerwald, M. L.; Nuckolls, C. Influence of molecular conformation on electron transport in giant, conjugated macrocycles. *J. Am. Chem. Soc.* **2018**, *140*, 10135–10139.

(28) Ball, M.; Zhang, B.; Zhong, Y.; Fowler, B.; Xiao, S.; Ng, F.; Steigerwald, M.; Nuckolls, C. Conjugated Macrocycles in Organic Electronics. *Acc. Chem. Res.* **2019**, *52*, 1068–1078.

(29) Darzi, E. R.; Hirst, E. S.; Weber, C. D.; Zakharov, L. N.; Lonergan, M. C.; Jasti, R. Synthesis, properties, and design principles of donor–acceptor nanohoops. *ACS Cent. Sci.* **2015**, *1*, 335–342.

(30) Kuwabara, T.; Orii, J.; Segawa, Y.; Itami, K. Curved Oligophenylenes as Donors in Shape-Persistent Donor–Acceptor Macrocycles with Solvatofluorochromic Properties. *Angew. Chem. Int. Ed.* **2015**, *54*, 9646–9649.

(31) Li, C.; Wang, C.; Guo, Y.; Jin, Y.; Yao, N.; Wu, Y.; Zhang, F.; Li, W. A

diketopyrrolopyrrole-based macrocyclic conjugated molecule for organic electronics. *J. Mater. Chem. C* **2019**, *7*, 3802–3810.

(32) Li, G.; Gopalakrishna, T. Y.; Phan, H.; Herng, T. S.; Ding, J.; Wu, J. From open-shell singlet diradicaloid to closed-shell global antiaromatic macrocycles. *Angew. Chem.* **2018**, *130*, 7284–7288.

(33) Ni, Y.; Gopalakrishna, T. Y.; Phan, H.; Kim, T.; Herng, T. S.; Han, Y.; Tao, T.; Ding, J.; Kim, D.; Wu, J. 3D global aromaticity in a fully conjugated diradicaloid cage at different oxidation states. *Nat. Chem.* **2020**, *12*, 242–248.

(34) Rickhaus, M.; Jirasek, M.; Tejerina, L.; Gotfredsen, H.; Peeks, M. D.; Haver, R.; Jiang, H.-W.; Claridge, T. D.; Anderson, H. L. Global aromaticity at the nanoscale. *Nat. Chem.* **2020**, *12*, 236–241.

(35) Liu, Y.; Phan, H.; Herng, T. S.; Gopalakrishna, T. Y.; Ding, J.; Wu, J. Toward Benzobis (thiadiazole)-based Diradicaloids. *Chem. Asian J.* **2017**, *12*, 2177–2182.

(36) Ni, Y.; Gopalakrishna, T. Y.; Wu, S.; Wu, J. A Stable All-thiophene-based Core-modified [38] Octaphyrin Diradicaloid: Conformation and Aromaticity Switch at Different Oxidation States. *Angew. Chem. Int. Ed.* **2020**, *59*, 7414–7418.

(37) Baird, N. C. Quantum organic photochemistry. II. Resonance and aromaticity in the lowest 3. pi.. pi.* state of cyclic hydrocarbons. *J. Am. Chem. Soc.* **1972**, *94*, 4941–4948.

(38) Fei, Z.; Han, Y.; Gann, E.; Hodsden, T.; Chesman, A. S.; McNeill, C. R.; Anthopoulos, T. D.; Heeney, M. Alkylated selenophene-based ladder-type monomers via a facile route for high-performance thin-film transistor applications. *J. Am. Chem. Soc.* **2017**, *139*, 8552–8561.

(39) Williams-Harry, M.; Bhaskar, A.; Ramakrishna, G.; Goodson, T.; Imamura, M.; Mawatari, A.; Nakao, K.; Enozawa, H.; Nishinaga, T.; Iyoda, M. Giant thienylene-

acetylene-ethylene macrocycles with large two-photon absorption cross section and semishape-persistence. *J. Am. Chem. Soc.* **2008**, *130*, 3252–3253.

(40) Darzi, E. R.; Jasti, R. The dynamic, size-dependent properties of [5]–[12] cycloparaphenylenes. *Chem. Soc. Rev.* **2015**, *44*, 6401–6410.

(41) Huang, H.; Yang, L.; Facchetti, A.; Marks, T. J. Organic and polymeric semiconductors enhanced by noncovalent conformational locks. *Chem. Rev.* **2017**, *117*, 10291–10318.

(42) Izumi, S.; Higginbotham, H. F.; Nyga, A.; Stachelek, P.; Tohnai, N.; de Silva, P.; Data, P.; Takeda, Y.; Minakata, S. Thermally Activated Delayed Fluorescent Donor–Acceptor–Donor–Acceptor π-Conjugated Macrocycle for Organic Light-Emitting Diodes. *J. Am. Chem. Soc.* **2020**, *142*, 1482–1491.

(43) Gibson, G. L.; McCormick, T. M.; Seferos, D. S. Atomistic band gap engineering in donor–acceptor polymers. *J. Am. Chem. Soc.* **2011**, *134*, 539–547.

(44) Lu, X.; Gopalakrishna, T. Y.; Phan, H.; Herng, T. S.; Jiang, Q.; Liu, C.; Li, G.; Ding, J.; Wu, J. Global Aromaticity in Macrocyclic Cyclopenta-Fused Tetraphenanthrenylene Tetraradicaloid and Its Charged Species. *Angew. Chem.* **2018**, *130*, 13236–13240.

(45) Schleyer, P. v. R.; Maerker, C.; Dransfeld, A.; Jiao, H.; van Eikema Hommes, N. J. Nucleus-independent chemical shifts: a simple and efficient aromaticity probe. *J. Am. Chem. Soc.* **1996**, *118*, 6317–6318.

(46) Geuenich, D.; Hess, K.; Köhler, F.; Herges, R. Anisotropy of the induced current density (ACID), a general method to quantify and visualize electronic delocalization. *Chem. Rev.* **2005**, *105*, 3758–3772.

(47) Klod, S.; Kleinpeter, E. Ab initio calculation of the anisotropy effect of multiple bonds and the ring current effect of arenesapplication in conformational and configurational analysis. *J. Chem. Soc., Perkin. Trans. 2* **2001**, 1893–1898.

(48) Lu, X.; Gopalakrishna, T. Y.; Han, Y.; Ni, Y.; Zou, Y.; Wu, J. Bowl-Shaped Carbon Nanobelts Showing Size-Dependent Properties and Selective Encapsulation of C70. *J. Am. Chem. Soc.* **2019**, *141*, 5934–5941.

(49) Sung, Y. M.; Yoon, M.-C.; Lim, J. M.; Rath, H.; Naoda, K.; Osuka, A.; Kim, D. Reversal of Hückel (anti) aromaticity in the lowest triplet states of hexaphyrins and spectroscopic evidence for Baird's rule. *Nat. Chem.* **2015**, *7*, 418.

(50) Jasti, R.; Bhattacharjee, J.; Neaton, J. B.; Bertozzi, C. R. Synthesis, characterization, and theory of [9]-,[12]-, and [18] cycloparaphenylene: carbon nanohoop structures. *J. Am. Chem. Soc.* **2008**, *130*, 17646–17647.

(51) Ono, K.; Tanaka, S.; Yamashita, Y. Benzobis (thiadiazole) s containing hypervalent sulfur atoms: novel heterocycles with high electron affinity and short intermolecular contacts between heteroatoms. *Angew. Chem. Int. Ed. Engl.* **1994**, *33*, 1977–1979.

(52) Frisch, M. J. et al. Gaussian 16 Revision B.01. 2016; Gaussian Inc. Wallingford CT.

(53) Becke, A. D. A new mixing of Hartree–Fock and local density-functional theories. *J. Chem. Phys.* **1993**, *98*, 1372–1377.

(54) Schuchardt, K. L.; Didier, B. T.; Elsethagen, T.; Sun, L.; Gurumoorthi, V.; Chase, J.; Li, J.; Windus, T. L. Basis set exchange: a community database for computational sciences. *J. Chem. Inf. Model.* **2007**, *47*, 1045–1052.

(55) Francl, M. M.; Pietro, W. J.; Hehre, W. J.; Binkley, J. S.; Gordon, M. S.; DeFrees, D. J.; Pople, J. A. Self-consistent molecular orbital methods. XXIII. A polarization-type basis set for second-row elements. *J. Chem. Phys.* **1982**, *77*, 3654–3665.

(56) Foresman, J. B.; Frisch, Æ. *Exploring Chemistry with Electronic Structure Methods*, 3rd ed.; Gaussian: Gaussian Inc. Wallingford CT, 2015.

(57) Noodleman, L. Valence bond description of antiferromagnetic coupling in transition metal dimers. *J. Chem. Phys.* **1981**, *74*, 5737–5743.

(58) Head-Gordon, M. Characterizing unpaired electrons from the one-particle density matrix. *Chem. Phys. Lett.* **2003**, *372*, 508–511.

(59) Schleyer, P. v. R.; Manoharan, M.; Wang, Z.-X.; Kiran, B.; Jiao, H.; Puchta, R.; van Eikema Hommes, N. J. Dissected nucleus-independent chemical shift analysis of π-aromaticity and antiaromaticity. *Org. Lett.* **2001**, *3*, 2465–2468.

(60) Ditchfield, R. Self-consistent perturbation theory of diamagnetism: I. A gauge-invariant LCAO method for NMR chemical shifts. *Mol. Phys.* **1974**, *27*, 789–807.

(61) Glendening, E. D.; Landis, C. R.; Weinhold, F. NBO 6.0: Natural bond orbital analysis program. *J. Comput. Chem.* **2013**, *34*, 1429–1437.

(62) Yanai, T.; Tew, D. P.; Handy, N. C. A new hybrid exchange–correlation functional using the Coulomb-attenuating method (CAM-B3LYP). *Chem. Phys. Lett.* **2004**, *393*, 51–57.

(63) Hirata, S.; Head-Gordon, M. Time-dependent density functional theory within the Tamm–Dancoff approximation. *Chem. Phys. Lett.* **1999**, *314*, 291–299.

(64) Tomasi, J.; Mennucci, B.; Cammi, R. Quantum mechanical continuum solvation models. *Chem. Rev.* **2005**, *105*, 2999–3094.